Available online at www.sciencedirect.com
ScienceDirect
Remote Sensing of Environment 104 (2006) 43–49
Remote Sensing of Environment
www.elsevier.com/locate/rse

Real-time monitoring and short-term forecasting of land surface phenology

Michael A. White [a,*], Ramakrishna R. Nemani [b]

[a] Department of Aquatic, Watershed, and Earth Resources, Utah State University, Logan, Utah, USA
[b] NASA Ames Research Center, Moffett Field, California, USA

Received 17 February 2006; received in revised form 28 April 2006; accepted 29 April 2006

Abstract

Land surface phenology is an important process for real-time monitoring and short-term forecasting in diverse land management, health, and hydrologic modeling applications. Yet current efforts to characterize phenological processes are limited by remote sensing challenges and lack of uncertainty estimates. Here, for a global distribution of phenologically and climatically similar phenoregions, we used the Advanced Very High Resolution Radiometer to develop a conceptually and computationally simple technique for real-time and forecast applications. Our overall approach was to analyze the phenological behavior of groups of pixels without recourse to smoothing or fitting. We used a 3-step initial process: (1) define a phenoregion specific normalized difference vegetation index threshold; (2) for all days from 1982–2003, calculate the percent of pixels above the threshold (PAT); (3) calculate daily 1982–2003 empirical distributions of PAT. For real-time monitoring, the current PAT may then be compared to the historical range of variability and visualized in relation to user-defined levels. Using similar concepts, we projected daily PAT up to one month in the future and compared predicted and actual dates at which a hypothetical PAT was reached. We found that the maximum lead-time of phenological forecasts could be analytically defined for user-specified uncertainty levels. The approach is adaptable to different remote sensing technologies and provides a foundation for ascribing a sequence of ground conditions (e.g. snowmelt, vegetative growth, pollen production, insect phenology) to remotely sensed land surface phenology observations.
© 2006 Elsevier Inc. All rights reserved.

Keywords: Growing season; Budburst; Bud break; Senescence; Spring; Fall

1. Introduction

Land surface phenology, defined as the seasonal pattern of variation in vegetated land surfaces observed from remote sensing, has been well-studied with historical remote sensing data (Jolly et al., 2005; Justice et al., 1985; Lloyd, 1990; Schwartz et al., 2002). Conversely, real-time or near real-time modeling and monitoring efforts are less well-served by current satellite remote sensing schemes. Diverse fields, such as fire forecasts (Roads et al., 2005), ecosystem forecasting (White & Nemani, 2004), insect pest phenology (Mussey & Potter, 1997), organism dispersal (Gage et al., 1999), agriculture (Mkhabela et al., 2005; Weissteiner & Kuhbauch, 2005), and health risk assessment (Traidl-Hoffmann et al., 2003) could benefit greatly from a conceptually, technically, and statistically simple land surface phenology monitor and forecasting technique. We submit that such an approach should include the following five principles.

1.1. Principle 1

Land surface phenology information should not be provided for individual pixels. Remote sensing provides a statistical distribution of a random variable, not an exact representation of the state of the land surface or atmosphere at a particular pixel. Additionally, assessing individual pixels in real-time presents nearly intractable problems of highly noisy timeseries without a globally defensible method to accept or reject rapid changes in the normalized difference vegetation index (NDVI, related to the fraction of photosynthetically active radiation absorbed by canopies, FPAR) or other remote sensing metrics.

* Corresponding author.

0034-4257/$ - see front matter © 2006 Elsevier Inc. All rights reserved.
doi:10.1016/j.rse.2006.04.014

1.2. Principle 2

Groups of phenologically and climatically similar pixels should be analyzed simultaneously as an empirical or statistical (e.g. Gaussian) distribution. When treated as a distribution, aberrant behavior by any one or several timeseries is irrelevant; no smoothing is required to reduce noise drastically.

1.3. Principle 3

Phenological timeseries should not be filled, fitted, or smoothed. Most existing phenological assessment methods, faced with the prospect of extremely noisy timeseries of remotely sensed data, often NDVI, smooth the data using one of many existing techniques (Jonsson & Eklundh, 2004). For a given date, these methods typically require looking both backwards and forwards in time, negating use in real-time or forecast applications. Further, many methods assume that a given mathematical function, such as piecewise logistic functions (Zhang et al., 2003), approximates true phenological development. In global, or even regional application this may be an untenable assumption, especially in cases of disturbance, defoliation, or NDVI curves with sharp peaks or broad plateaus (Potter et al., 2003).

1.4. Principle 4

The continual process of land surface phenology development, not just dates of specific events, such as the start of spring or fall, should be described. Unlike in traditional ground-based phenology research, in which a date may be recorded for budburst (Chuine, 2000) or flowering (Thórhallsdóttir, 1998), land surface phenology is the integral of a continuum of processes including snowmelt, changes in soil wetness, and multiple non-coincident vegetation development patterns (de Beurs & Henebry, 2004). Consequently, the global relationships between remotely sensed land surface phenology and particular plant-based events are generally unknown.

1.5. Principle 5

Measures of variability and/or uncertainty should be included. For monitoring applications, variability measures will allow the user to distinguish between an unusual event and an event within the normal range of variability. For land surface phenology forecasting, knowledge of historical variability is critical.

Our goal is to combine these five principles in a new land surface phenology monitoring and forecasting technique. In the following sections, we use a historical NDVI global remote sensing dataset to present (1) the monitoring methodology for an example region and (2) the forecasting methodology for both an example region and a global distribution of pixel groups.

2. Data

In support of Principles 1 and 2 — monitoring should be conducted for groups of pixels not single pixels — we used the phenoregion map of White et al. (2005) to identify groups of related pixels. To create the 500 phenoregions, White et al. (2005) first used a wavelet analysis to identify pixels with a consistently strong annual amplitude in 8 km Advanced Very High Resolution Radiometer (AVHRR) NDVI and then used an Oak Ridge National Laboratory supercomputer to create pixel clusters with similar phenological and climatic cycles (phenoregions available online at http://www.daac.ornl.gov/). For demonstration purposes, we randomly selected a phenoregion in eastern Canada (Fig. 1).

For methodological development and the forecasting example, we obtained continental 8 km resolution 15-day maximum value composited Global Inventory Modeling and Mapping Studies (GIMMS) NDVI (Pinzon et al., 2005) (available online at www.landcover.org). We reprojected the data into the global interrupted

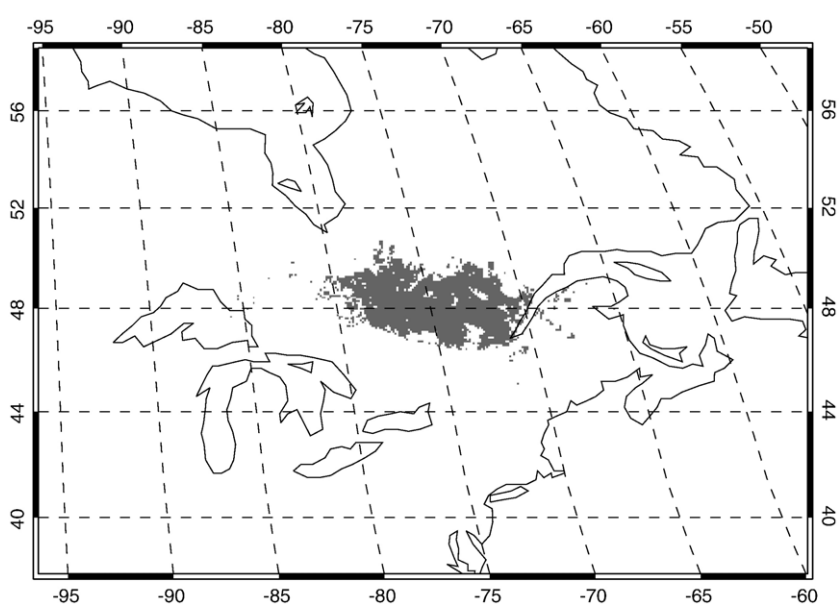

Fig. 1. Demonstration phenoregion in eastern Canada.

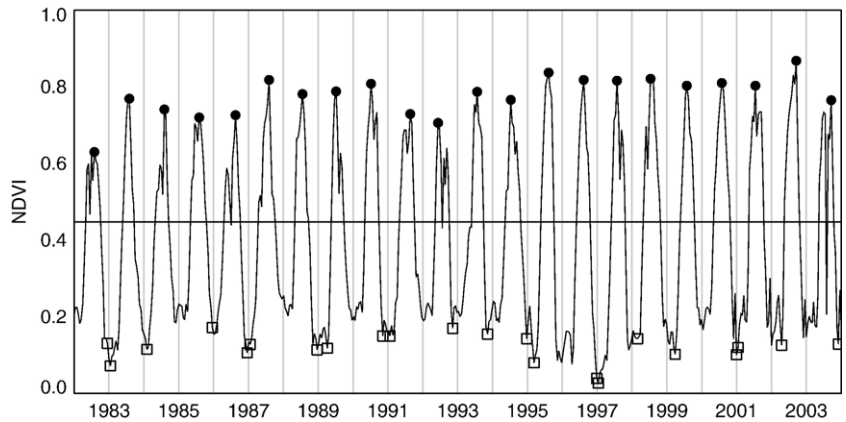

Fig. 2. Random pixel from demonstration phenoregion showing the calculation of the NDVI threshold. Circles show annual maximum NDVI; open squares are annual minimum NDVI; horizontal line is the NDVI threshold midway between the average minimum and maximum NDVI.

Goode's Homolosine projection used for the phenoregion analysis.

3. Methods

Using the following three steps, we developed a method for real-time or near real-time land surface phenology monitoring: (1) selecting an NDVI threshold; (2) calculating, on a daily basis, the percent of a phenoregion above the threshold; and (3) calculating the deviation of real-time phenology from the long-term phenological development pattern.

3.1. Selecting thresholds

Analytical change detection methods, such as derivatives, are plagued by the high frequency variability present in nearly all NDVI timeseries. Given the wide variability in NDVI amplitude, a globally constant NDVI threshold is also unusable: a threshold of 0.2, for example, may be appropriate for some forested ecosystems but may exceed the peak NDVI of some semi-arid grasslands (White et al., 2003). Thus, we calculated absolute but phenoregion-specific NDVI threshold as follows.

For every pixel in each phenoregion (3013 for the demonstration phenoregion in Fig. 1) we extracted the 1982–2003 annual minimum and maximum NDVI and, from these 22 values, calculated the long-term average minimum and maximum NDVI. We then calculated the NDVI threshold as the value halfway between the minimum and maximum, which generally corresponds to the time of maximum NDVI increase and decrease (White et al., 1997). From the distribution of NDVI thresholds for every pixel in the phenoregion, we calculated the phenoregion mean threshold and 95% confidence interval of the mean.

3.2. Daily percent above the threshold

There are two GIMMS NDVI values per month; we assigned the early composite to the 1st day of the month and the late composite to the 15th day of the month. We then linearly interpolated daily NDVI values for each pixel in the phenoregion. This step is in technical violation of Principle 3 (no filling, fitting, or smoothing) but the daily GIMMS NDVI are used here for proof-of-concept development meant to represent the temporal resolution of impending continental-scale rolling composite datasets in which each day is the maximum value of the previous days (as in production by the Earth Resources Observation Systems Data Center for the Moderate Resolution Imaging Spectroradiometer (MODIS) over the conterminous USA). For every day, we calculated the percent of pixels above the phenoregion NDVI threshold, hereafter referred to as the percent above threshold (PAT).

3.3. Deviations from historical patterns

For yeardays 1–365, we calculated the interquartile range of 1982–2003 PAT. Use of the Gaussian approximation was untenable, especially for spring growth phases in which the 1982–2003 distribution was highly non-normal, and we opted for the empirical distribution. We then visualized each day from 1982–2003 as to whether or not it was an unusually low (below the 25th percentile) or high (above the 75th percentile) PAT condition.

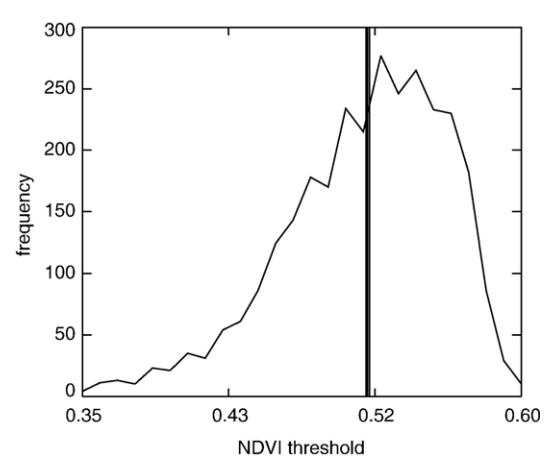

Fig. 3. Frequency distribution of NDVI threshold values for the demonstration phenoregion. Vertical lines show the phenoregion mean NDVI threshold and 95% confidence interval (lines overlap the mean).

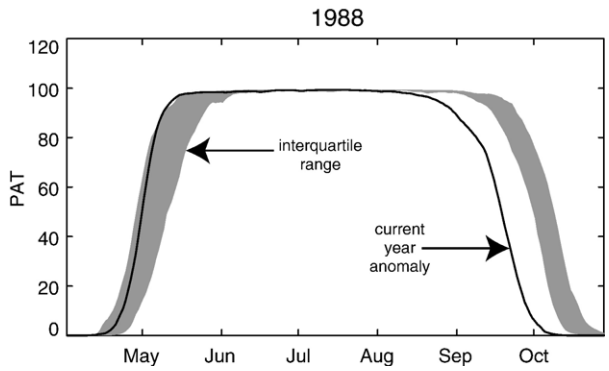

Fig. 4. Implementation scheme for real-time monitoring. Shaded region shows the 1982–2003 interquartile range of PAT. Thick solid line shows the 1988 PAT. From mid-August to mid-October, the 1988 PAT was below the 25th percentile.

While the definition of low/high and the selection of visualization technique is subjective, the ability to represent a continual process of real-time phenological development relative to long-term average conditions is not. Specific approaches may be customized for famine, pollen, irrigation, or other phenologically sensitive applications.

3.4. Forecasting

Land surface phenology forecasts are inherently use-specific. Trace gas purposes, for example, are likely to be quite different than pollen forecasting needs. A universally applicable approach for describing uncertainty in land surface phenology forecasts therefore does not exist. Instead, we demonstrate a hypothetical example in which the user wishes to forecast the date at which PAT exceeds 50, i.e. at least half of the pixels in the phenoregion are above the threshold. We term this date PAT50. Further, the hypothetical user is willing to accept a 2-day uncertainty, as measured by the mean absolute error (MAE) of prediction. We established the maximum forecast leadtime for the global phenoregion distribution as follows.

First, we developed a phenoregion-specific daily lookup table containing, for each day, a sorted listing of 1982–2003 PAT values. Beginning on January 1, 1982, we established the ranking

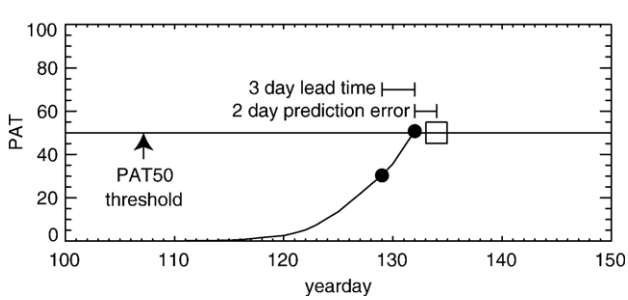

Fig. 5. Forecasting approach. On every yearday, forecasts with leadtimes from 1 to 31 days are made; if the forecast predicts PAT exceeding the PAT50 threshold, the current leadtime and prediction error are recorded. Left filled circle shows the current yearday; right filled circle shows yearday at which PAT50 was predicted to be exceeded; open square shows yearday when true PAT50 was exceeded.

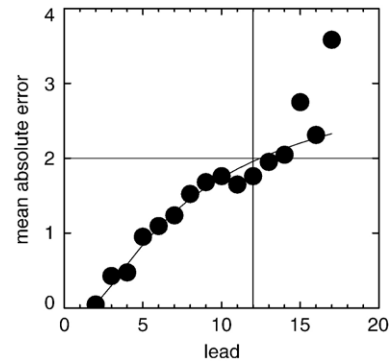

Fig. 6. Mean absolute error for forecasts of PAT50 in the demonstration phenoregion as a function of forecast lead. Errors increased as a function of longer lead. Eq. (3) was used to fit a weak exponential function; Eq. (5) was used to invert the equation to solve for the maximum allowable leadtime (vertical line) for a 2-day allowable error (horizontal line).

of the current day's PAT within the sorted long-term values and projected this relative position 31 days into the future. If the forecast included an occurrence of a day with PAT greater than or equal to 50 preceded by values less than 50 PAT, we recorded this date as the predicted PAT50. For example, on May 1, 1982 in the demonstration phenoregion, the PAT of 27 was the 9th record in the sorted 1982–2003 lookup table. The 9th position was then forecasted from the lookup table for May 2 to June 2, generating a PAT50 prediction on May 6. We recorded the forecast lead-time from the current day i and predicted PAT50 as:

$$\text{lead} = \text{PAT50}_{\text{pred}} - i \tag{1}$$

and the forecast error as:

$$\text{absolute error} = |\text{predicted PAT50} - \text{observed PAT50}| \tag{2}$$

For each phenoregion, we then extracted all errors at each unique lead (possible leads 1 to 31 days). For all leads we calculated the mean absolute error and the 95% confidence interval. We removed individual leads with less than 10 values, indicating rare predictions, and phenoregions with less than 3 unique leads, indicating generally unpredictable conditions. Exploratory scatter plots indicated 2 general relationships between lead and mean absolute error: weak exponential and linear. Therefore, using lead as the explanatory $\boldsymbol{x}$ vector, mean absolute error as the response $\boldsymbol{y}$ vector, and the 95% confidence interval as the $\boldsymbol{y}$ vector uncertainty, we used a Levenberg–Marquardt least-squares fit (IDL function mpfitexpr.pro derived from MINPACK-1; available from http://cow.physics.wisc.edu/~craigm/idl/idl.html) to fit the functions

$$\text{mean absolute error} = \exp^{\frac{\beta_0}{\text{lead}}}\beta_1 + \beta_2 \tag{3}$$

and

$$\text{mean absolute error} = \beta_0 \text{lead} + \beta_1 \tag{4}$$

For each phenoregion, we selected Eq. (3) or Eq. (4) based on lowest mean absolute residuals. Depending on the selection

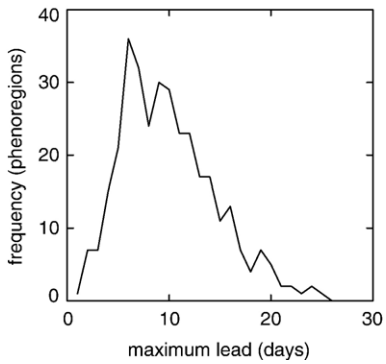

Fig. 7. Global phenoregion frequency distribution of maximum forecast leadtime when the user is willing to accept a 2-day mean absolute error.

of exponential or linear function, we solved for the allowable lead for predicting PAT50 ($PAT50_{lead}$) with a 2-day mean absolute error by inverting Eq. (3):

$$PAT50_{lead} = \frac{\beta_0}{\ln\left(\frac{\text{mean absolute error} - \beta_2}{\beta_1}\right)} \quad (5)$$

or Eq. (4):

$$PAT50_{lead} = \frac{\text{mean absolute error} - \beta_1}{\beta_0} \quad (6)$$

Operationally, the hypothetical user would take a specified action only if the predicted PAT50 occurred within the $PAT50_{lead}$ defined analytically for the phenoregion in use.

4. Results

4.1. Monitoring

From a random pixel within the demonstration phenoregion (Fig. 1), the NDVI threshold, based on the annual minimum and maximum NDVI values, was 0.45 (Fig. 2). From the distribution of the 3013 NDVI thresholds in the phenoregion (Fig. 3), the mean NDVI threshold was 0.51 ± 0.002 (95% confidence interval).

Graphical presentation of daily PAT relative to the historical interquartile range allowed for simple assessment of abnormal land surface phenology conditions. In an example year of 1988 (Fig. 4), PAT was within the interquartile range until mid-August when a persistent low anomaly began and persisted until mid-October.

4.2. Forecasting

For the demonstration phenoregion (Fig. 1), mean absolute error increased with leadtime (Fig. 5) with increasing scatter at leadtime longer than two weeks. Inverting the exponential function (Eq. (5)) produced $PAT50_{lead}$ of 12 days for the 2-day allowable mean absolute error (Fig. 6). For the global distribution of phenoregions, mean $PAT50_{lead}$ was seven days for a 2-day allowable mean absolute error (Fig. 7).

5. Discussion

Our results show that real-time monitoring of land surface phenology may be conducted in four central steps: (1) identify groups of phenologically and climatically similar pixels: (2) analyze pixel distributions to develop location-specific thresholds; (3) construct long-term NDVI (or related metric) empirical distributions; and (4) assess real-time land surface phenology estimates as a continual measure of deviation from long-term conditions. Based on this process, it is then practicable to generate a forecasting scheme in which the user may specify a maximum allowable error that is then translatable into a maximum allowable land surface phenology forecast leadtime. While the datasets and methods employed here are appropriate for proof-of-concept development, other applications will mandate use-specific approaches and/or different remote sensing platforms, as discussed below.

The phenoregion dataset used in this study is based on global coarse-resolution datasets (White et al., 2005). For implementation, we anticipate that users will generate clusters at a spatial resolution appropriate for their application. For the conterminous US, for example, a reclustering based on MODIS land surface temperature (Wan et al., 2002) and vegetation indices (Huete et al., 2002) is planned for the Terrestrial Observation and Prediction System (White & Nemani, 2004). The phenoregion dataset used also does not allow for shifting distributions related to climate, landuse, and/or landcover changes. We suggest two methods to account for shifting phenoregion distributions. (1) Analyze multi-year trends in PAT percentiles averaged over individual months. Systematically increasing or decreasing PAT percentiles may indicate a land surface phenology shift away from long-term mean patterns, thus necessitating a reclustering. (2) Annually redefine the location of pixels nearest to cluster centers. In this approach, cluster definitions are constant but cluster locations are allowed to shift dynamically. If sub-phenoregion resolution is desired, we recommend that the user subdivide the phenoregion based on the spatial variability in the timing of PAT50 or similar event.

The selection of the threshold midway between the minimum and maximum NDVI is designed to correspond to the period of maximum NDVI increase and decrease (White et al., 1997) but in reality, there is no data to link quantitatively any satellite threshold or other detection technique to global patterns of surface vegetation phenology, which is often considerably different that land surface phenology. In northern ecosystems the dominant annual cycle and consequent threshold selection is often controlled by an annual snow cycle superimposed on limited canopy variability. In other ecosystems, the annual cycle may be dominated by cloudy and clear cycles. Even in deciduous systems where senescent vegetation is coincident with snow cover, NDVI relationships to vegetation seasonality may be temporally variable (Wang et al., 2005). Although local solutions are possible (Delbart et al., 2005), assuming that land surface phenology corresponds directly to vegetation phenology is fraught with difficulties. Fortunately, use of phenoregions provides an ideal geographic basis with which to assess the correspondence of the phenoregion NDVI threshold to ground conditions. In these cases users may find a higher or lower threshold derived from within-phenoregion distributions (Fig. 2) to be appropriate for a particular application.

Ascribing a globally consistent biological definition to the PAT metric or events such as PAT50 is also difficult. It is tempting to state, for example, that when PAT50 is reached, the phenoregion has greened up or that the growing season has begun. Yet, as stated previously, this may simply represent snowmelt with no change in the vegetation canopy. Ideal implementation of the PAT monitoring technique should therefore focus on relating PAT progressions to abiotic and biotic processes within the phenoregion. For example, in a hypothetical phenoregion, the following may occur: snowmelt at 20 PAT; understory herbaceous growth at 40 PAT; deciduous leaf out at 60 PAT; crop emergence at 80 PAT. Continuous tracking of an integrative metric such as PAT should allow for relating remote sensing to a continual process of land surface phenology change instead of a single date extraction.

Phenoregion-specific land surface phenology variability is an especially critical component of forecasting applications. Our approach, based on either percentiles or forecasts of sorted PAT values, does not rely on distribution assumption. However, we completed a similar forecasting approach based on the Gaussian approximation and forecasts of current anomalies calculated from the mean and standard deviations; results were extremely similar with a mean global forecast leadtime of six days, as opposed to seven days with the sorted PAT approach. The approach thus appears to be resistant to use of modeled versus empirical distributions. For specific regions or applications, distribution analysis and selection may still be appropriate, though.

Other forecasting approaches have been developed, especially for agricultural applications (Ji & Peters, 2004; Kaitho et al., 2003) and with use of autoregressive moving average models. These approaches have been successful but rely on location specific parameter fitting (Ji & Peters, 2004) or have been designed to forecast future forage conditions based on current NDVI (Kaitho et al., 2003). Our approach is generic and, to our knowledge, no other approach has provided management ability to specify an allowable error and to then invert a maximum forecast leadtime.

Exceptions to our principles and forecasting approach certainly exist. In deciduous canopies without significant snow and cloud cover and when using a rigorously georectified remote sensing product, it may be practicable to analyze individual pixels. For homogenous regions, especially crops, forecasting using plant growth models coupled with real-time remote sensing and meteorological forecasts may be superior to the empirical approach outlined above.

6. Conclusions

We present a generally applicable methodology for real-time monitoring and short-term forecasting of land surface phenology. The method is conceptually and computationally simple, avoids problems related to processing phenological metrics for individual pixels in real-time, and allows users to specify measures of statistical uncertainty. In real-time, users may visually interpret phenological development relative to historical variability of an empirical pixel distribution. In forecast mode and using a proof-of-concept dataset, we showed that a hypothetical land surface phenology event could be predicted with a lead-time of 7 days for an allowable prediction uncertainty of 2 days.

Acknowledgements

Support was provided by NASA grant NAG5-11282 (MAW) and the NASA ESE (RRN).

References

Chuine, I. (2000). A unified model for budburst of trees. *Journal of Theoretical Biology*, *207*, 337−347.

de Beurs, K. M., & Henebry, G. M. (2004). Land surface phenology, climatic variation, and institutional change: Analyzing agricultural land cover change in Kazakhstan. *Remote Sensing of Environment*, *89*, 497−509.

Delbart, N., Kergoat, L., Le Toan, T., Lhermitte, J., & Picard, G. (2005). Determination of phenological dates in boreal regions using normalized difference water index. *Remote Sensing of Environment*, *97*, 26−38.

Gage, S. H., Isard, S. A., & Colunga, M. (1999). Ecological scaling of aerobiological dispersal processes. *Agricultural and Forest Meteorology*, *97*, 249−261.

Huete, A., Didan, K., Miura, T., Rodriguez, E. P., Gao, X., & Ferreira, L. G. (2002). Overview of the radiometric and biophysical performance of the MODIS vegetation indices. *Remote Sensing of Environment*, *83*, 195−213.

Ji, L., & Peters, A. (2004). Forecasting vegetation greenness with satellite and climate data. *IEEE Geoscience and Remote Sensing Letters*, *1*, 3−6.

Jolly, W. M., Nemani, R., & Running, S. W. (2005). A generalized, bioclimatic index to predict foliar phenology in response to climate. *Global Change Biology*, *11*, 619−632.

Jonsson, P., & Eklundh, L. (2004). TIMESAT — A program for analyzing time-series of satellite sensor data. *Computers & Geosciences*, *30*, 833−845.

Justice, C. O., Townshend, J. R. G., Holben, B. N., & Tucker, C. J. (1985). Analysis of the phenology of global vegetation using meteorological satellite data. *International Journal of Remote Sensing*, *6*, 1271−1318.

Kaitho, R., Stuth, J., Angerer, J., Jama, A., Mnene, W., Kingamkono, M. et al. (2003). A new system to forecast near-term forage conditions for early warning systems in pastoral regions of East Africa. Research Brief 03-02-LEWS, Global Livestock Collaborative Research Support Program, Davis, CA.

Lloyd, D. (1990). A phenological classification of terrestrial vegetation cover using shortwave vegetation index imagery. *International Journal of Remote Sensing*, *11*, 2269−2279.

Mkhabela, M. S., Mkhabela, M. S., & Mashinini, N. N. (2005). Early maize yield forecasting in the four agro-ecological regions of Swaziland using NDVI data derived from NOAAs-AVHRR. *Agricultural and Forest Meteorology*, *129*, 1−9.

Mussey, G. J., & Potter, D. A. (1997). Phenological correlations between flowering plants and activity of urban landscape pests in Kentucky. *Journal of Economic Entomology*, *90*, 1615−1627.

Pinzon, J., Brown, M. E., & Tucker, C. J. (2005). EMD correction of orbital drift artifacts in satellite data stream. In N. Huang, & S. Shen (Eds.), *The Hilbert–Huang transform and its applications* (pp. 167−183). Hackensack, NJ: World Scientific Publishing Co.

Potter, C., Tan, P. N., Steinbach, M., Klooster, S., Kumar, V., Myneni, R., et al. (2003). Major disturbance events in terrestrial ecosystems detected using global satellite data sets. *Global Change Biology*, *9*, 1005−1021.

Roads, J., Fujioka, F., Chen, S., & Burgan, R. (2005). Seasonal fire danger forecasts for the USA. *International Journal of Wildland Fire*, *14*, 1−18.

Schwartz, M. D., Reed, B., & White, M. A. (2002). Assessing satellite-derived start-of-season (SOS) measures in the conterminous USA. *International Journal of Climatology*, *22*, 1793−1805.

Thórhallsdóttir, T. E. (1998). Flowering phenology in the central highland of Iceland and implications for climatic warming in the arctic. *Oecologia*, *114*, 43−49.

Traidl-Hoffmann, C., Kasche, A., Menzel, A., Jakob, T., Thiel, M., Ring, J., et al. (2003). Impact of pollen on human health: More than allergen carriers? *International Archives Of Allergy and Immunology*, *131*, 1−13.

Wan, Z., Zhang, Y., Li, Z. -L., Wang, R., Salomonson, V. V., Yves, A., et al. (2002). Preliminary estimate of calibration of the Moderate Resolution Imaging Spectroradiometer (MODIS) thermal infrared data using Lake Titicaca. *Remote Sensing of Environment*, *80*, 497−515.

Wang, Q., Adiku, S., Tenhunen, J., & Granier, A. (2005). On the relationship of NDVI with leaf area index in a deciduous forest site. *Remote Sensing of Environment*, *94*, 244−255.

Weissteiner, C. J., & Kuhbauch, W. (2005). Regional yield forecasts of malting barley (*Hordeum vulgare* L.) by NOAA-AVHRR remote sensing data and ancillary data. *Journal of Agronomy and Crop Science*, *191*, 308−320.

White, M. A., Brunsell, N., & Schwartz, M. D. (2003). Vegetation phenology in global change studies. In M. D. Schwartz (Ed.), *Phenology: An integrative environmental science* (pp. 453−466). New York, NY: Kluwer Academic Publishers.

White, M. A., Hoffman, F., Hargrove, W. W., & Nemani, R. R. (2005). A global framework for monitoring phenological responses to climate change. *Geophysical Research*, 32.

White, M. A., & Nemani, R. R. (2004). Soil water forecasting in the continental United States: Relative forcing by meteorology versus leaf area index and the effects of meteorological forecast errors. *Canadian Journal of Remote Sensing*, *30*, 717−730.

White, M. A., Thornton, P. E., & Running, S. W. (1997). A continental phenology model for monitoring vegetation responses to interannual climatic variability. *Global Biogeochemical Cycles*, *11*, 217−234.

Zhang, X. Y., Friedl, M. A., Schaaf, C. B., Strahler, A. H., Hodges, J. C. F., Gao, F., et al. (2003). Monitoring vegetation phenology using MODIS. *Remote Sensing of Environment*, *84*, 471−475.